



1 **Cloud top pressure retrieval with DSCOVR-EPIC oxygen A and B bands observation**

2 Bangsheng Yin¹, Qilong Min^{1,*}, Emily Morgan¹, Yuekui Yang², Alexander Marshak², and
3 Anthony B. Davis³

4

5 ¹Atmospheric Sciences Research Center, University at Albany, Albany, NY, USA

6 ²NASA Goddard Space Flight Center, Climate and Radiation Laboratory, Greenbelt, MD,
7 USA

8 ³Jet Propulsion Laboratory, California Institute of Technology, Pasadena, CA, USA

9

10

11 * Corresponding author, qmin@albany.edu

12

13 **Abstract**

14 An analytic transfer model for Earth Polychromatic Imaging Camera (EPIC) observation
15 was proposed to retrieve the cloud top pressure (CTP) with considering in-cloud photon
16 penetration. In this model, an analytic equation was developed to represent the reflection at top
17 of atmosphere (TOA) from above cloud, in-cloud and below-cloud. The coefficients of this
18 analytic equation can be derived from a series of EPIC simulations under different atmospheric
19 conditions using a non-linear regression algorithm. With estimated cloud pressure thickness, the
20 CTP can be retrieved from EPIC observation data by solving the analytic equation. To simulate
21 the EPIC measurements, a program package using the double-*k* approach was developed, which
22 can calculate high-accuracy results with a one-hundred-fold time reduction. During the retrieval
23 processes, two kinds of retrieval results, i.e., baseline CTP and retrieved CTP, are provided. The
24 baseline CTP is derived without considering in-cloud photon penetration, and the retrieved CTP
25 is derived by solving the analytic equation, taking into consideration the in-cloud and below-
26 cloud interactions. The retrieved CTP for the oxygen A and B bands are smaller than their
27 related baseline CTP. At the same time, both baseline CTP and retrieved CTP at the oxygen B-
28 band are obviously larger than those at the oxygen A-band. Compared to the difference of
29 baseline CTP between the B-band and A-band, the difference of retrieved CTP between these
30 two bands is generally reduced.

31

32 **1. Introduction**

33 The Deep-Space Climate Observatory (DSCOVR) satellite is an observation platform
34 orbiting within the first Sun-Earth Lagrange point (L1), 1.5 million km from the Earth, carrying a
35 suite of instruments oriented both Earthward and sunward. One of the Earthward instruments is
36 the Earth Polychromatic Imaging Camera (EPIC) sensor. The EPIC continuously monitors the
37 entire sunlit Earth for backscatter from sunrise to sunset with 10 narrowband filters: 317, 325,
38 340, 388, 443, 552, 680, 688, 764 and 779 nm (Marshak *et al.*, 2018). Of the 10 narrow-band
39 channels, there are two oxygen absorption and reference pairs, 764nm versus 779.5nm and
40 680nm versus 687.75nm, for oxygen A and B bands. The cloud top pressure (CTP) or cloud top



41 height (CTH) is an important cloud property for climate and weather studies. Based on
42 differential oxygen absorption, both EPIC oxygen A-band and B-band pairs can be used to
43 retrieve CTP. It is worth noting that although CTP and CTH reference the same characteristic of
44 clouds, the conversion between the two depends on their atmospheric profiles.

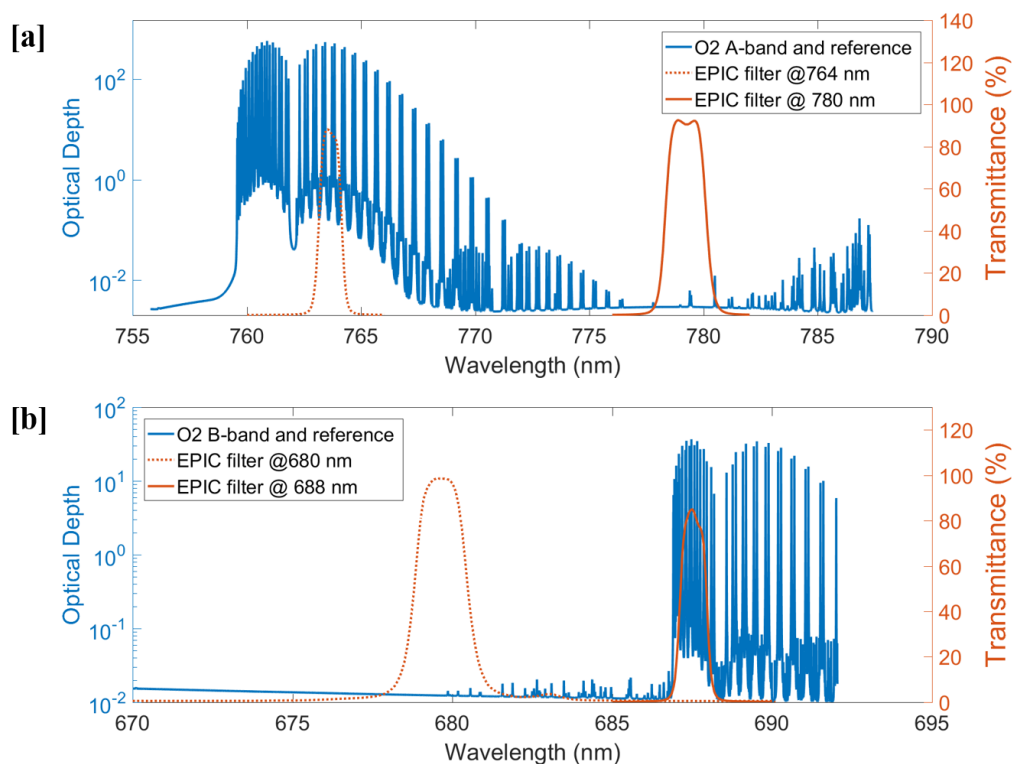
45 Although the theory of using oxygen absorption bands to retrieve CTP was proposed
46 decades ago, it is still very challenging to do the retrieval accurately due to the complicated in-
47 cloud penetration effect (*Yang et al., 2019, 2013; Davis et al., 2018a, 2018b; Schuessler et al.,*
48 *2013; Kuze and Chance, 1994; O'brien and Mitchell, 1992; Fischer and Grassl, 1991; and etc.*).
49 Many approaches are designed to retrieve clouds' effective top pressures without considering
50 their in-cloud photon penetration, and therefore derive effective top pressures higher than CTP.
51 Currently, the Atmospheric Science Data Center (ASDC) at National Aeronautics and Space
52 Administration (NASA) Langley Research Center archives both calibrated EPIC reflectance ratio
53 data and processed Level 2 cloud retrieval products, including cloud cover, cloud optical depth,
54 cloud effective top pressure at oxygen A and B bands (*Yang et al., 2019*).

55 In this paper, to address the issue of in-cloud penetration, we proposed an analytic method
56 to retrieve the CTP by using DSCOVR EPIC oxygen A- and B-band observation. The structure
57 of this paper is as follows: section 2 describes the absorption optical depth spectrum at oxygen A
58 and B bands with their related DSCOVR EPIC filters, section 3 states the theory of CTP retrieval
59 based on EPIC oxygen A-band and B-band observation, section 4 describes the retrieval
60 algorithms in detail with case studies and examples of global observation data retrieval, and
61 section 5 states the conclusions of this study.

62

63 2. DSCOVR EPIC oxygen A and B bands filters

64 EPIC filters at 764 nm and 779 nm cover the oxygen A-band absorption and reference
65 band, respectively (Figure 1a). In this wavelength range, the O₃ absorption is very weak (O₃
66 optical depth < 0.003) and there are no other gas absorptions. The background aerosol and
67 Rayleigh scattering optical depth vary smoothly within the A-band range; the differences
68 between in-band and reference band are negligible. EPIC filters at 688 nm and 680 nm cover the
69 oxygen B-band absorption and reference band, respectively (Figure 1b). Compared to the oxygen
70 A-band, O₃ absorption is slightly stronger in the oxygen B-band range, with an O₃ optical depth
71 around 0.01. Any water vapor absorption in the B-band range is negligible. In the standard
72 atmospheric model, from the oxygen B-band reference band to the absorption band, the O₃
73 absorption and Rayleigh scattering optical depth decreased by approximately 0.0002 and 0.002,
74 respectively. This may have some impacts on the CTP retrieval from the oxygen B-band (more
75 discussion in the later sections).



76
77

78 **Figure 1:** High resolution calculated absorption optical depth spectrum at oxygen A-band (a)
79 and B-band (b) with DSCOVER EPIC oxygen A and B bands in-band and reference filters.

80 In general, if we use the pair of oxygen A and B absorption and reference bands together,
81 the impact of other absorption lines, background Rayleigh scattering, and aerosol optical depth
82 are very limited. At the same time, as a well-mixed major atmospheric component, the vertical
83 distribution of oxygen in the atmosphere is very stable under varying atmospheric conditions.
84 Thus, we can use the ratio of reflected radiance (or reflectance) at the top of atmosphere (TOA)
85 of oxygen absorption and reference bands to study the photon path length distribution and derive
86 the cloud information. Also, the ratios of absorption/reference are less impacted by the
87 instrument calibration and other measurement error.

88

89 3. Theory of CTP retrieval based on EPIC oxygen A- and B- band observation

90

91 In our study, we tried two methods to retrieve the CTP based on EPIC oxygen A-band and
92 B-band measurements: (1) Build a lookup table (LUT) for various atmospheric conditions and do
93 the retrieval by searching the LUT; (2) Develop an analytic transfer model for EPIC observations
94 and calculate the related coefficients based on a series of simulated values, then use this analytic
95 transfer model to retrieve the CTP. In this paper, we mainly focus on the second method.

96 3.1 Method 1: LUT based approach



97 One commonly used method of retrieval for satellite observation is through the building
98 and usage of LUTs. For DSCOVER EPIC observations, we can build a LUT by simulating the
99 EPIC measurements under various atmospheric conditions, such as different surface albedo,
100 solar zenith and viewing angles, cloud optical depth, CTP and cloud pressure thickness. During
101 the retrieval process, the EPIC measurements (e.g., reflectance at oxygen A and B bands) with
102 related solar zenith and viewing angles can be obtained from the EPIC level 1B data; cloud
103 optical depth information (retrieved from other EPIC channels) can be obtained from EPIC level
104 2 data. At the same time, we can get surface albedo from Global Ozone Monitoring Experiment
105 2 (GOME-2) Surface Lambertian-equivalent reflectivity (LER) data (Tilstra *et al.*, 2017). At this
106 point the CTP and cloud pressure thickness are the only unknown variables. Cloud pressure
107 thickness can be estimated with cloud optical thickness using statistical rules. A multi-variable
108 LUT searching method can then be used to interpolate and obtain the CTP. It is worth noting that
109 certain variables will have a non-linear effect on EPIC observations, however, these variations
110 occur smoothly. With a relatively high-resolution simulated table, we can use a localized linear
111 interpolation method to estimate the proper values. Multiple interpolations are needed for this
112 method to decrease the number of LUT dimensions, which will cost more time than the analytic
113 transfer model method. The retrieval error of this method is determined by the resolution of the
114 LUT. In physics, the retrieval accuracy is impacted by two main uncertainty sources: (1) the
115 limited ability of EPIC in identifying cloud thermodynamic phase, which will affect the accuracy
116 of cloud optical thickness retrieval, and 2) the uncertainty in estimating Cloud pressure.

117 **3.2 Method 2: Analytic transfer model**

118 For a long time, various efforts have been devoted to the study of radiative transfer in the
119 atmosphere, including scattering, absorption, emission, and etc. (Chandrasekhar, 1960; Irvine
120 1964; Ivanov and Gutshabash 1974; van de Hulst 1980, 2012; Ishimaru, 1999; Thomas and
121 Stamnes, 2002; Davis and Marshak, 2002; Kokhanovsky *et al.*, 2003; Marshak and Davis, 2005;
122 Pandey *et al.*, 2012; and etc.). In this study, we are trying to develop an analytic radiative
123 transfer equation to analyze the radiative transfer at oxygen A and B bands. Through solving the
124 analytic equation, we can retrieve the CTP information directly. The theory of CTP retrieval is
125 similar for EPIC oxygen A-band and B-band observation. Here we use oxygen A-band as an
126 example to study the radiative transfer model. For oxygen A-band, photon path length
127 distribution is capable of describing vital information related to a variety of cloud and
128 atmospheric characteristics.

$$129 \quad I_v(\mu, \varphi; \mu_0, \varphi_0) = I_0(\mu, \varphi; \mu_0, \varphi_0) \int_0^\infty p(l, \mu, \varphi; \mu_0, \varphi_0) e^{-\kappa_v l} dl \quad (1)$$

130 Where, $p(l)$ is photon path length distribution, κ_v is the gaseous absorption coefficient, $\mu =$
131 $\cos(\theta)$, $\mu_0 = \cos(\theta_0)$, $(\theta, \varphi; \theta_0, \varphi_0)$ are zenith and azimuth angles for solar and sensor view
132 respectively, I_0 and I_v are incident solar radiation and sensor measured solar radiation,
133 respectively.

134 When clouds exist, the incident solar radiation is reflected to outer space in three primary
135 ways. First, incident solar radiation is reflected by cloud top layer directly as a result of single
136 scattering. Second, the incident solar radiation will penetrate into the cloud and be reflected back
137 to TOA through cloud top via multiple scattering. Third, the incident solar radiation will pass



138 through the cloud and arrive at the surface, after that it is reflected back into the cloud and finally
 139 scattered back to TOA through the cloud top. Due to the position of the EPIC instrument and the
 140 long distance between EPIC and Earth, we can consider that solar zenith angle and sensor view
 141 angle are nearly reverse. At oxygen A-band, the reflected solar radiation will be reduced due to
 142 oxygen absorption depending on photon path length distributions. Absorption is negligible in
 143 oxygen A-band's reference band. For solar radiation at oxygen A-band and its reference band,
 144 they are also attenuated by air mass and aerosol that located above or below cloud through
 145 Rayleigh scattering and aerosol extinction. However, their attenuations from Rayleigh scattering
 146 and aerosol extinction are close to each other. Thus, we can use the ratio of EPIC measured
 147 reflectance at oxygen A-band and its reference band to derive the photon path length distribution,
 148 and then retrieve cloud information such as CTP.

149 To simplify the analytic transfer model for EPIC observation, we made a series of
 150 assumptions, e.g., isotropic component, a plane-parallel assumption with quasi-Lambertian
 151 reflecting surfaces, and etc. In this model, μ and μ_0 are the same as in Equation 1, φ is the
 152 relative azimuth angle between solar and satellite sensors; A_{surf} is the surface albedo; $t_{O_2}^{Top}$, $t_{O_2}^{Base}$,
 153 and $t_{O_2}^{Surface}$ are oxygen A-band absorption optical depth from TOA to cloud top layer, cloud
 154 bottom layer, and surface, respectively; $\Delta t_{O_2}^{Above-Cloud}$, $\Delta t_{O_2}^{In-Cloud}$ and $\Delta t_{O_2}^{Below-Cloud}$ are layered
 155 oxygen A-band absorption optical depth above cloud, in cloud, and below-cloud, respectively;
 156 functions f mean their contribution to the ratio of measured reflectance at oxygen A-band (R_A)
 157 and reference band (R_f). The detailed analysis of EPIC analytic transfer model is shown as
 158 follows:

159 (1) **Above Cloud:** the reflected solar radiation is determined by the oxygen absorption optical
 160 depth above the cloud and air mass directly.

$$161 \quad f(\Delta t_{O_2}^{Above-Cloud}, \mu_0, \mu, \varphi) = f(\Delta t_{O_2}^{Above-Cloud})f(\mu_0, \mu, \varphi)$$

$$162 \quad = t_{O_2}^{Top} \left(\frac{1}{\mu} + \frac{1}{\mu_0} \right) \quad (2)$$

163 (2) **Within Cloud:** the reflected solar radiation is not only determined by oxygen absorption
 164 optical depth above cloud and in-cloud, but also by penetration related factors, e.g., cloud optical
 165 depth. Due to photon penetration, oxygen parameter $t_{O_2}^{Top}$ influences the enhanced path length
 166 absorption:

$$167 \quad \Delta t_{O_2}^{In-Cloud} = t_{O_2}^{Base} - t_{O_2}^{Top} \quad (3)$$

168 Equivalence theorem (Irvine, 1964; Ivanov and Gutshabash, 1974; van de Hulst 1980) is used to
 169 separate absorption from scattering:

$$170 \quad f(t_{O_2}^{Top}, \Delta t_{O_2}^{In-Cloud}, \mu_0, \mu, \varphi) = f(t_{O_2}^{Top}, \Delta t_{O_2}^{In-Cloud})f(\mu_0, \mu, \varphi)$$

$$171 \quad = f(t_{O_2}^{Top})f_1(\mu_0, \mu, \varphi) + f(\Delta t_{O_2}^{In-Cloud})f_2(\mu_0, \mu, \varphi) \quad (4)$$

172 $f(t_{O_2}^{Top})$ is determined by two absorption dependences: strong ($\sim \sqrt{t_{O_2}^{Top}}$) and weak ($\sim t_{O_2}^{Top}$).

$$173 \quad f(t_{O_2}^{Top}) = a_1 \sqrt{t_{O_2}^{Top}} + b_1(t_{O_2}^{Top}) \quad (5)$$



174 Based on asymptotic approximation (Kokhanovsky *et al.*, 2003; Pandey *et al.*, 2012), the
 175 reflection of a cloud without considering below cloud interaction is given by Equation 6:

$$176 \quad R(t, \mu, \mu_0, T) = R_0^\infty(t, \mu, \mu_0) - TK(\mu)K(\mu_0)$$

$$177 \quad = R_0^\infty(t, f_1(\mu, \mu_0)) - Tf_2(\mu, \mu_0) \quad (6)$$

178 Here, R_0^∞ is the reflectance of a semi-infinite cloud, $K(\mu)$ is the escape function of μ , T is global
 179 transmittance of a cloud. T can be estimated by Equation 7, with the cloud optical thickness τ_{cld} ,
 180 the asymmetry parameter g , and $\alpha = 1.07$ a numerical constant.

$$181 \quad T = \frac{1}{0.75\tau_{cld}(1-g)+\alpha} \quad (7)$$

182 f_1 and f_2 functions have a quadratic form as follows:

$$183 \quad f_{i-1} = a_i T + b_i(\mu + \mu_0) + c_i T(\mu + \mu_0) + d_i \mu \mu_0, i = 2,3 \quad (8)$$

184 Combining Equations 4, 5 and 8, we can get the equation 9:

$$185 \quad f(t_{O2}^{Top}, \Delta t_{O2}^{cld}, \mu_0, \mu, \varphi) = \left(a_1 \sqrt{t_{O2}^{Top}} + b_1(t_{O2}^{Top}) \right) (a_2 T + b_2(\mu + \mu_0) + c_2 T(\mu + \mu_0) + d_2 \mu \mu_0)$$

$$186 \quad + \Delta t_{O2}^{n-cloud} (a_3 T + b_3(\mu + \mu_0) + c_3 T(\mu + \mu_0) + d_3 \mu \mu_0) \quad (9)$$

187

188 (3) **Below Cloud:** The equivalence theorem used for below cloud is similar to within cloud
 189 (Kokhanovsky *et al.*, 2003; Pandey *et al.*, 2012).

$$190 \quad f(\Delta t_{O2}^{Below-Cld}, \mu_0, \mu, \varphi) = T t_{O2}^{Surface} \frac{A_{Surf}}{1+(e_4 * T + f_4) * A_{Surf}}$$

$$191 \quad * (a_4 T + b_4(\mu + \mu_0) + c_4 T(\mu + \mu_0) + d_4 \mu \mu_0) \quad (10)$$

192

193 Combining Equations 2, 9 and 10, we can get the total EPIC analytic transfer equation as
 194 follows:

$$195 \quad -\log\left(\frac{R_A}{R_f}\right) = f(\Delta t_{O2}^{Above-Cld}, \mu_0, \mu, \varphi) + f(t_{O2}^{Top}, \Delta t_{O2}^{cld}, \mu_0, \mu, \varphi) + f(\Delta t_{O2}^{Below-Cld}, \mu_0, \mu, \varphi) \quad (11)$$

196 In this total analytic equation, there are 16 coefficients ($a_1, b_1, a_2, \dots, d_4, e_4, f_4$), which can
 197 be calculated through nonlinear regression algorithm according to a series of simulated values
 198 for different atmospheric conditions. Based on Equation 11, we can finally obtain a quadratic

199 equation, $A\sqrt{t_{O2}^{Top}^2} + B\sqrt{t_{O2}^{Top}} + C = 0$, where the parameters A, B and C (not shown here) can be
 200 derived from Equation 11 directly. When these parameters (i.e., A, B and C) are obtained from
 201 EPIC observation data and other data source, we can easily solve the quadratic equation to
 202 retrieve cloud top O2 absorption depth, and then CTP.

203 4. Detailed retrieval algorithm

204 As previously stated, in method 2, the analytic EPIC equation (i.e., Equation 11) is key for
 205 the CTP retrieval. To derive the coefficients of Equation 11, a series of model simulations for



206 various atmospheric conditions are needed. Thus, developing a radiative transfer model to
207 simulate the EPIC measurements at A- and B-bands and their reference bands is the first thing
208 we need to complete.

209 **4.1 Oxygen A- and B-band absorption coefficients calculation**

210 To simulate the EPIC measurements, one of the most important steps is calculating
211 oxygen absorption coefficients at oxygen A-band and B-band. In this step, the latest HITRAN
212 database (*Gordon et al., 2017*) is used to provide the absorption parameters, and the LBLRTM
213 package (*Clough et al., 2005*) is used to calculate oxygen absorption coefficients layer by layer.
214 In our algorithm, the whole Earth atmosphere is divided by 63 layers.

215 Since oxygen absorption coefficients are pressure (or pressure-squared) and temperature
216 dependent, and the lines are well fitted as Lorentzian in the lower atmosphere, the relationship
217 can be written as follows:

$$218 \quad k_i = \frac{S_i}{\pi} \frac{\alpha_i}{(v-v_i)^2 + \alpha_i^2} \quad (12)$$

$$219 \quad \alpha_i = \alpha_i^0 \frac{p}{p_0} \left(\frac{T_0}{T}\right)^{\frac{1}{2}}, \quad S_i = S(T_0) \frac{T_0}{T} \exp\left[1.439E\left(\frac{1}{T_0} - \frac{1}{T}\right)\right] \quad (13)$$

220 Where S_i is the line intensity, v_i and α_i are the line center wave number and half width,
221 respectively; p_0 and T_0 are standard atmospheric pressure and temperature, respectively.

222 An unfortunate result of this is that cloud levels at a given pressure-weighted oxygen
223 absorption depth can have drastically different heights depending on the atmospheric profile in
224 use. We have used the LBLRTM package to calculate oxygen parameters for each
225 pressure/temperature profile; a time-consuming process. Our goal has been to find a simple and
226 fast conversion function from pressure to altitude for different atmospheric profiles. Using a
227 polynomial fitting function, fitting coefficients can be determined for oxygen absorption and
228 applied to any given atmosphere [*Min et al., 2014; Chou and Kouvaris, 1986*].

$$229 \quad A_{vLM} = [a_0(v, P) + a_1(v, P) \times (T_{LM} - T_{mL}) + a_2(v, P) \times (T_{LM} - T_{mL})^2] \times \rho_{O_2} \quad (14)$$

230 Where A_{vLM} is optical depths for layer L, spectral point v, and atmosphere model M; ρ_{O_2} is
231 molecular column density ($\frac{\text{molecules}}{\text{cm}^2} \times 10^{-23}$); T_{LM} is the average temperature for layer L for a
232 given atmosphere; and T_{mL} is average temperature over all atmospheres (M1 to M6) for layer L.
233

234 **4.2 Fast radiative transfer model for simulating high-resolution oxygen A- and B-bands**

235 We cannot simply calculate narrowband mean optical depth and then calculate the radiation
236 for various atmospheric conditions when simulating EPIC narrowband measurements. The
237 correct way is described as follows: firstly, simulate the solar radiation spectrum $S(k(\lambda))$ under
238 specific atmospheric conditions, then integrate the spectrum with EPIC narrowband
239 filter $R(k(\lambda))$ to obtain simulated narrowband measurements (Equation 15).

$$240 \quad R(\lambda) = \int S(k(\lambda))R(k(\lambda))d\lambda \neq R(\overline{k(\lambda)}) \quad (15)$$

241 With the high spectrum resolution oxygen absorption coefficient data, we can simulate the
242 high resolution upward diffuse oxygen A-band or B-band spectrum through DISORT code



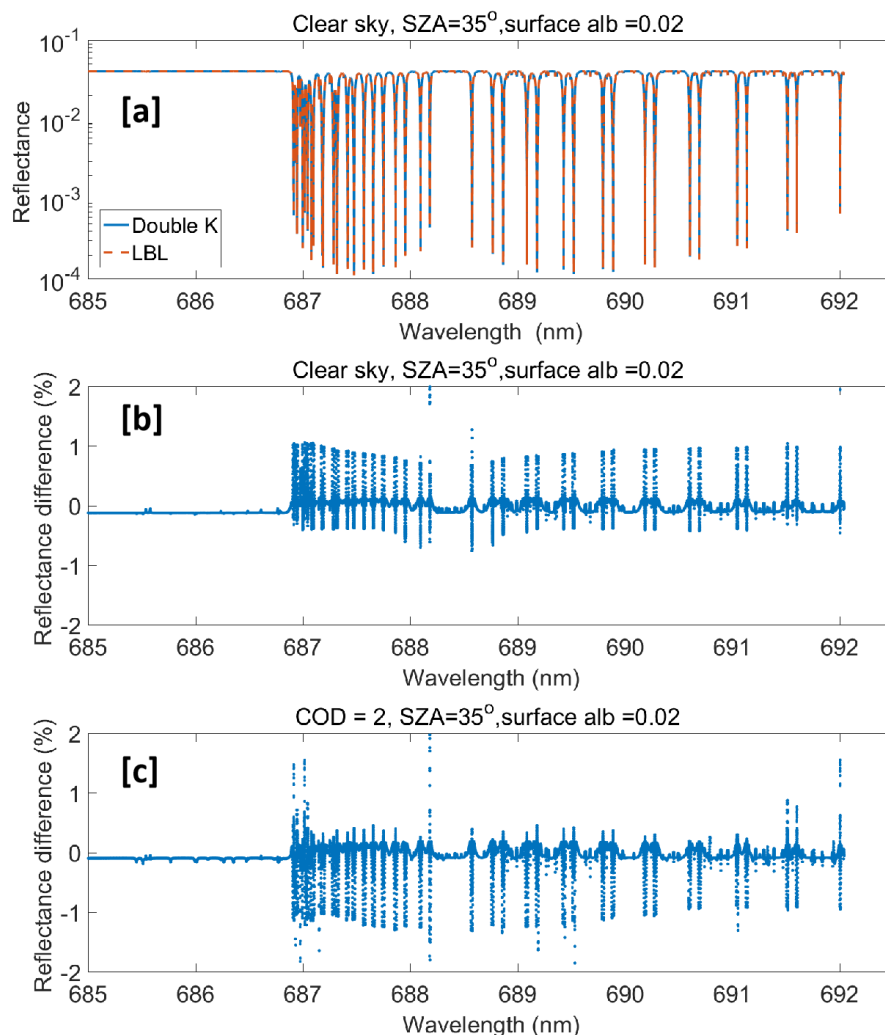
243 (*Stamnes et al., 1988*) for any given atmospheric condition, which has various surface albedo,
244 SZA, cloud optical depth, cloud top height (pressure), and cloud geometric (pressure) thickness.
245 However, due to the high spectrum resolution, it is very time-consuming when performing line
246 by line (LBL) calculations. Thus, developing a fast radiative transfer model for simulating high
247 resolution oxygen A-band and B-band spectrum is necessary.

248 In this project, the double- k approach is used to develop a fast radiative transfer model for
249 oxygen A-band and B-band respectively. [*Min and Harrison 2004; Duan et al, 2005*] proposed
250 a fast radiative transfer model. In their approach, the radiation from absorption and scattering
251 processes of cloud and aerosol are split into the single- and multiple-scattering components: The
252 single scattering component is computed line-by-line (LBL), while multiple scattering (second
253 order and higher) radiance is approximated.

$$\begin{aligned} 254 \quad I &= I^{ss}(\lambda) + I^{ms}(\lambda) \\ 255 \quad &\approx I^{ss}[Z^h(p, t), P^h, \lambda] + I^{ms}[Z^h(p, t), P^h, \lambda] \\ 256 \quad &\approx I^{ss}[Z^h(p, t), P^h, \lambda] + I^{ms}[Z^l(p, t), P^l, \lambda] \\ 257 \quad &\approx I^{ss}[Z^h(p, t), P^h, \lambda] + I^{ms}\{F[Z^l(p, t), P^l, k(\lambda_i)]\} \end{aligned} \quad (16)$$

258 Equation 16 is from Equation 1 in Duan et al. (2005): ss and ms mean single and multiple scattering,
259 respectively. Z is the optical properties of the atmosphere as a function of pressure p and
260 temperature t , with P being the phase function of that layer. H and L represent higher and lower
261 number of layers and streams, respectively. F is the transform function between wave number
262 space and k space, defined from a finite set of $k(\lambda_i)$.

263 The application of Double- k approach in oxygen A-band has been presented in detail in
264 Duan et al. 2005. Here we take oxygen B-band as an example. The detailed fast radiative transfer
265 model for simulating high-resolution oxygen B-band is as follows: The first order scattering
266 radiance is calculated accurately by using a higher number of layers and streams for all required
267 wavenumber grid points. The multiple-scattering component is extrapolated and/or interpolated
268 from a finite set of calculations in the space of two integrated gaseous absorption optical depths
269 to the wavenumber grids: a double- k approach. The double- k approach substantially reduces the
270 error due to the uncorrelated nature of overlapping absorption lines. More importantly, these
271 finite multiple-scattering radiances at specific k values are computed with a reduced number of
272 layers and/or streams in the forward radiative transfer model. To simulate an oxygen B-band
273 spectrum with high accuracy, 33 k values and 99 calculations of radiative transfer are chosen in
274 our program. This results in around a hundred-fold time reduction with respect to the standard
275 forward radiative transfer calculation.



276

277 **Figure 2.** [a] High resolution reflectance at EPIC O2 B-Band simulated by fast radiative model
278 (double-k) and benchmark (LBL); Difference between simulated reflectance by double-k and
279 LBL for a clear sky case [b] and a cirrus cloud case with COD=2 [c]. Here SZ=35°, surface albedo = 0.02.
280

281 As shown in Figure 2, under clear sky and thin cloud situations, the simulated high
282 resolution upward diffuse oxygen B-band spectra from LBL calculation and double-k approach
283 are compared. The spectrum difference between LBL calculation and double-k approach is very
284 small and hard to tell directly (Figure 2a). Under both situations, most of the relative difference
285 between these two methods are under 0.5%. The obvious relative difference (>1%) occurs only
286 in the wavelength range with high absorption optical depth, which has little contribution to the
287 integrated solar radiation. Therefore, for the simulated narrowband measurements at EPIC
288 oxygen B-band, the relative difference between LBL and double-k approach is much smaller



289 than that of the high resolution spectrum, which is less than 0.1% for both clear day and cloud
 290 situations (shown in Table 1). For optically thick cloud situations, the accuracy of the double-k
 291 approach is similar to that of thin cloud situations.

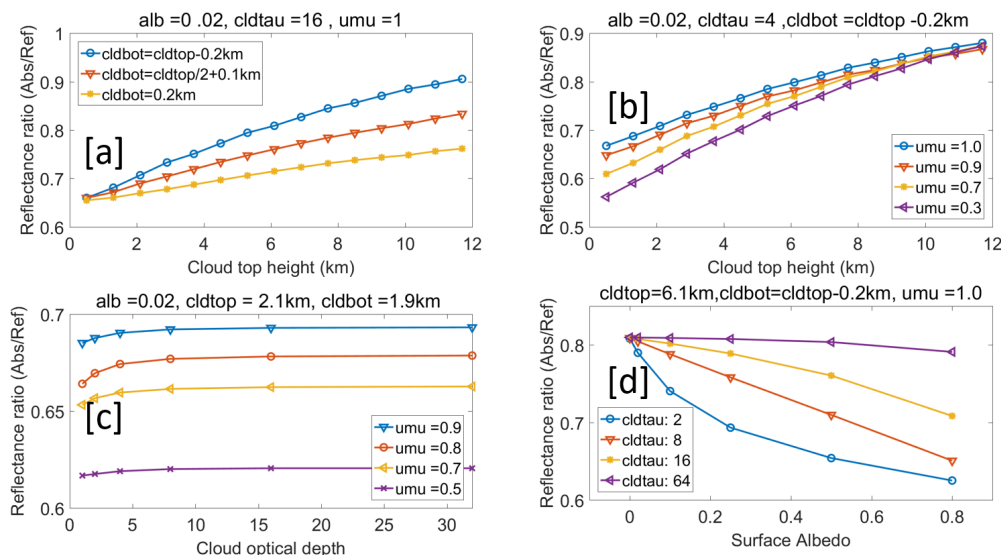
292 **Table 1.** Comparison of simulated narrowband measurement at EPIC B-Band channel

Case	Line by line	Double-k	Difference
Clear day	0.026963	0.026985	+0.08%
Thin Cloud	0.084046	0.084033	-0.02%

293

294 4.3 Simulation of oxygen A- and B-bands for different atmospheric conditions

295 Using the EPIC measurement simulation package, we made a series of simulations with
 296 different settings for surface albedo, solar zenith angle, cloud optical depth, cloud top height
 297 (pressure), and cloud geometric (pressure) thickness (or cloud bottom height). The results of
 298 these simulations consist of a data table, which can be used not only to calculate the coefficients
 299 for the analytic equation, but also to study the sensibility of every variant.



300

301 **Figure 3.** Ratio of simulated reflectance measurements for EPIC B-band to B-band reference
 302 with different surface albedo, cloud optical depth, solar zenith angle, cloud top height and cloud
 303 bottom height.

304 According to the previous theory study, the ratio of reflectance radiance (i.e., absorption
 305 to the reference) at TOA is determined by the photon path length distribution at oxygen A/B
 306 bands: the larger the mean photon path length, the stronger the absorption, and the smaller the
 307 reflectance ratio. To make the figures easy to view and understand, we use cloud top and bottom
 308 geometric height to represent cloud top pressure and thickness information in Figure 3. As
 309 shown in Figure 3a, the ratio of upward diffuse at oxygen B-band and its reference band is
 310 sensitive to the cloud top height (pressure). The higher the cloud top height, the larger the ratio.
 311 At the same time, this ratio is affected by the cloud bottom height (or cloud geometric thickness)



312 when the other cloud parameters are fixed, the lower the cloud bottom (or the larger the cloud
313 geometric thickness), the smaller the ratio. It is consistent with the theory analysis: (1) the higher
314 the cloud top height, the shorter the mean photon path length, and the weaker the absorption; (2)
315 when the cloud optical depth is given, larger cloud geometric thickness means smaller cloud
316 density, then the sunlight can penetrate deeper into the cloud, which results in a longer mean
317 photon path length. In Figure 3b, for clouds with given cloud top height, cloud optical depth and
318 geometric thickness, the ratio decreases with the solar and view angles. This is easy to
319 understand: the larger the solar and view angles, the longer the mean photon pathlength, and the
320 stronger the absorption. In Figure 3c, for clouds with given cloud top height and geometric
321 thickness, when the cloud optical depth is small (e.g., COD <5), the reflectance ratio increases
322 with cloud optical depth. However, when cloud optical depth is larger than 16, the effect of cloud
323 optical depth is small. This is because the larger the cloud optical depth, the shallower the
324 sunlight penetration, and the shorter the mean photon pathlength. In Figure 3d, for clouds with
325 given cloud optical depth, CTP, and geometric thickness, the ratio decreases with surface albedo.
326 The smaller the cloud optical depth, the stronger the impact of the surface albedo. This is
327 because the heavy cloud prevents the incident sunlight from passing through it to reach the
328 surface, and also prevents the reflected light from going back to the TOA.

329 For oxygen A-band, the ratio of upward diffuse at absorption and reference bands shows
330 similar characteristics as oxygen B-band. Compared to oxygen B-band, under the same
331 atmospheric conditions, the oxygen absorption at A-band is stronger, and the ratio of A-band to
332 its reference band has smaller values.

333 4.4 Case studies of cloud top pressure retrieval

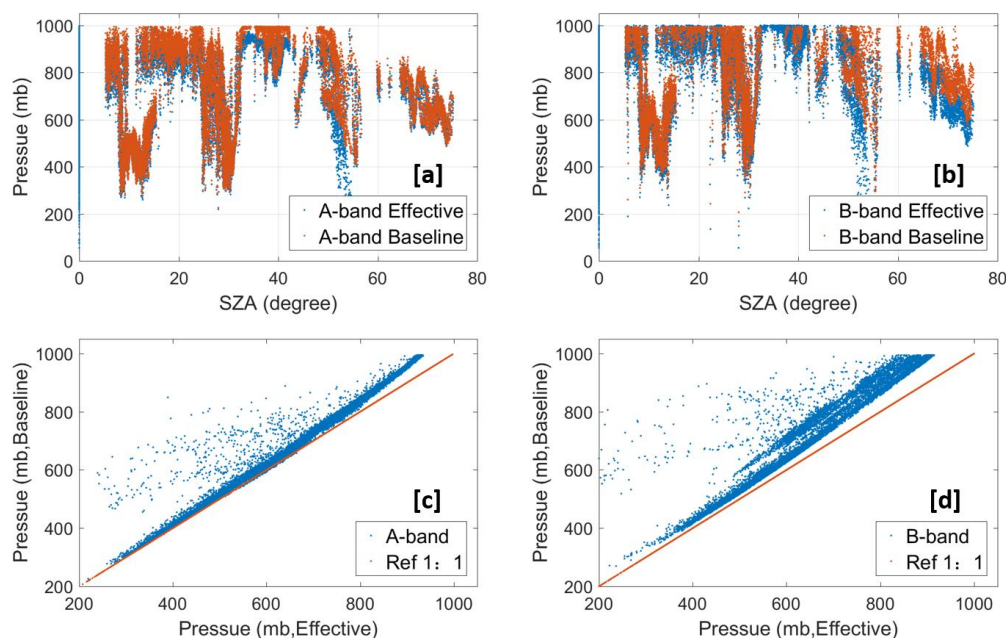
334 In our retrieval algorithm, we have two kinds of retrieval results: baseline CTP and retrieved
335 CTP. The baseline CTP is used as a reference for the retrieved CTP. It is similar to the effective
336 CTP in Yang et al., (2013), which does not consider cloud penetration. The retrieved CTP is
337 calculated by the analytic equation, which considers the in-cloud and below-cloud interaction.

338 During the baseline CTP calculation, the impact of penetration in-cloud is ignorable, and the
339 incident light reached cloud top is assumed reflected back directly. As shown in Equation 15, the
340 baseline absorption optical depth τ_{base} is derived from the ratio of upward diffuse at absorption
341 bands and their reference bands directly. According to the model calculated oxygen A and B
342 bands absorption optical depth profile at the specific solar zenith angle, the baseline CTP can be
343 derived directly.

$$344 \quad \tau_{base} = \log \left(-\frac{R_{abs}}{R_{ref}} \right) / \left(\frac{1}{\cos(\theta_{sza})} + \frac{1}{\cos(\theta_{view})} \right) \quad (15)$$

345 As shown in Figure 4, the baseline CTP value at A-band is slightly higher than the effective
346 CTP from NASA ASDC L2 data. But the baseline CTP value at B-band is substantially higher
347 than the effective CTP from NASA ASDC L2 data. The difference may be mainly from the
348 calculation of oxygen A and B bands absorption coefficients or the absorption optical depth
349 profile.

350



351
352

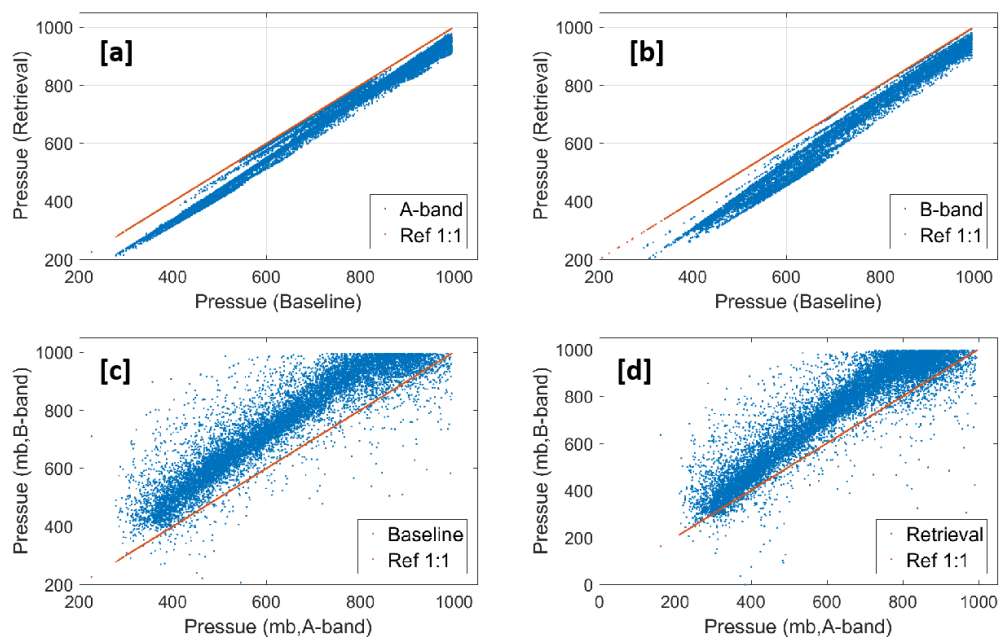
353 **Figure 4.** The comparison of effective CTP (reference from NASA ASDC data) and baseline
354 values from our retrieval algorithm for EPIC A and B bands.

355 Based on the simulated reflectance ratio under different atmospheric conditions, we can
356 calculate the coefficients for the analytic radiative transfer equations by using a nonlinear fitting
357 algorithm. The coefficients for different SZA's are calculated individually to reduce the fitting
358 error. Based on the calculated coefficients, we can retrieve the CTP with DISCOVER EPIC
359 observation data at oxygen A and B bands.

360 During the CTP retrieval, with the exception of the previously mentioned analytic
361 equation coefficients, we can get the surface albedo data from GOME, obtain reflectance data,
362 solar zenith and view angles, cloud optical depth, etc. from the NASA ASDC data file. Another
363 very important step in the retrieval processing is the acquisition of cloud pressure thickness data,
364 which has a substantial impact on the retrieval results. We currently use a statistical approach
365 (i.e., cloud pressure thickness (mb) = 2.5* cloud optical depth +26) to estimate the cloud
366 pressure thickness based on cloud optical depth. As shown in Figure 5a and 5b, the retrieved
367 CTP when considering cloud penetration is smaller than baseline CTP. For this case, the mean
368 difference between baseline CTP and retrieved CTP for oxygen A-band and B-bands are around
369 57 mb and 85 mb, respectively, which is consistent with theoretical expectations. For clouds with
370 a given CTP, the mean photon path length will increase substantially when considering cloud
371 penetration and interaction. A decrease in retrieved CTP will result in order to match the
372 measurement ratio of absorption to reference. Compared to the O2 A-band, both baseline CTP
373 and retrieved CTP for the O2 B-band are larger (Figure 5c and 5d). This is because the
374 absorption of solar radiation in the O2 B-band is weaker than that of the O2 A-band, and the
375 incident light at oxygen B-band can penetrate deeper into the cloud, allowing more light to pass



376 through. The difference in retrieved CTP between B band and A band (approx. 101 mb) is
377 generally reduced in comparison to baseline B band and A band (approx. 129 mb). This
378 indicates, as expected, more photon penetration correction for B-band than A-band.



379
380 **Figure 5.** (a and b) The comparison of retrieved CTP and baseline values for EPIC A and B
381 bands; (c and d) the comparison of retrieved CTP and baseline values between EPIC A- and B-
382 bands.

383 We also used the LUT based method to do the retrieval for the same observation data,
384 because both methods share the same EPIC simulation package and the same simulated data
385 table, the results of which are similar.

386

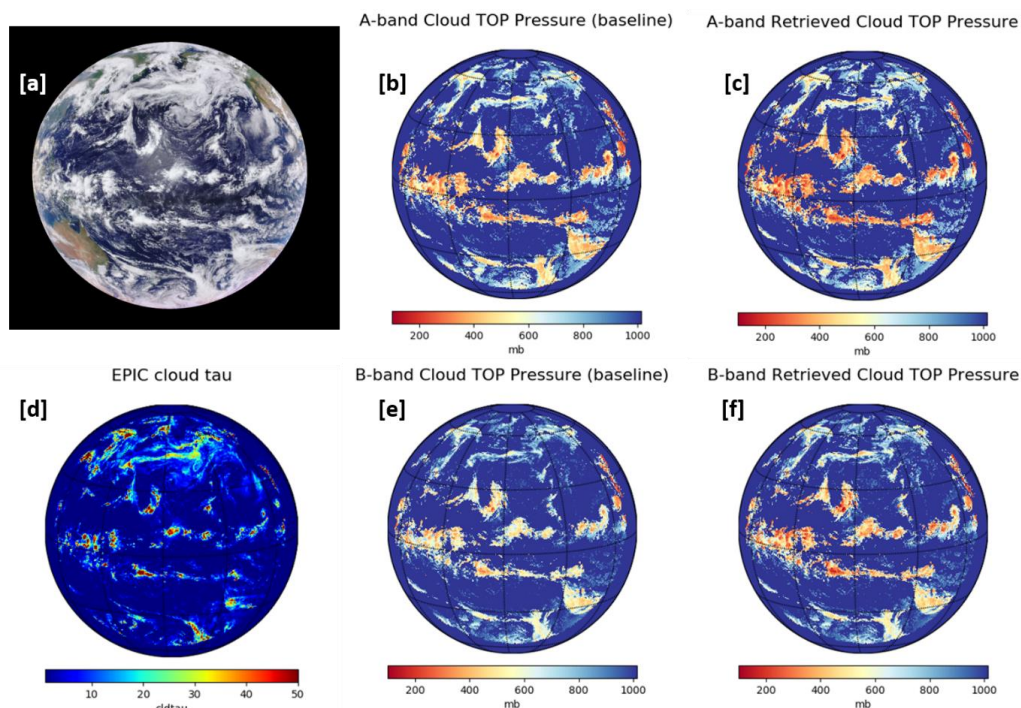
387 4.5 Retrieval of global observation

388 We applied our retrieval algorithm on the global DISCOVER EPIC measurement data at
389 oxygen A and B bands. During the retrieval, only pixels with total cloud covering (i.e., cloud
390 mask index of 4), surface albedo < 0.25, and cloud optical depth ≥ 3 are considered. To make
391 the picture easy to visualize, we set all invalid values to 1013; same as the background sea level
392 pressure.

393 Figure 6a shows the synthesized RGB picture of EPIC measurements at GMT time 00:17:51
394 on July 25, 2016. At this point in time the sun light covers most of the Pacific Ocean. In this
395 figure, the white pixels represent cloud cover. Figure 6d shows the global cloud optical depth
396 (NASA ASDC L2 data), which highlights areas consistent with the RGB image. Figure 6b and
397 6c show the baseline and retrieved CTP at A-band, respectively, which also highlights areas
398 (white to brown) consistent with the RGB image. Figure 6e and 6f show the baseline and
399 retrieved CTP in B-band respectively, which are similar to, but greater than the A-band. Because



400 we use the cloud optical depth to estimate the cloud pressure thickness in our retrieval, part of
401 the retrieval error is from the cloud optical depth and the equation for cloud pressure thickness
402 estimation.



403
404

405 **Figure 6.** (a) RGB image from DSCOVR EPIC measurement at GMT time 00:17:51 on July 25,
406 2016; (b) and (c) Baseline and retrieved CTP derived from EPIC A-band measurement. (d)
407 Cloud optical depth (liquid assumption) from EPIC L2 products; (e) and (f) Baseline and
408 retrieved CTP derived from EPIC B-band measurement.

409

410 5 Conclusion

411 The in-cloud photon penetration has significant impacts on the CTP retrieval when using
412 DSCOVR EPIC oxygen A- and B- band measurements. To address this issue, we proposed two
413 methods, (1) the LUT based method and (2) the analytic transfer model method for CTP retrieval
414 with consideration of in-cloud photon penetration. In the analytic transfer model method, we
415 build an analytic equation that represents the reflection at TOA from above cloud, in-cloud, and
416 below-cloud, respectively. The coefficients of this analytic equation can be derived from a series
417 of EPIC simulations under different atmospheric conditions using a non-linear regression
418 algorithm. With EPIC observation data, the related solar zenith and sensor view angle, surface
419 albedo data, cloud optical depth, and estimated cloud pressure thickness, we can retrieve the CTP
420 by solving the analytic equation.



421 We developed a package for the DSCOVR EPIC measurement simulation. The high
422 resolution radiation spectrum must be simulated first and then integrated with the EPIC filter
423 function in order to accurately simulate EPIC measurements. Because this process is highly time-
424 consuming, a polynomial fitting function is used when calculating the oxygen absorption
425 coefficients under different atmospheric conditions. At the same time, the double-k approach is
426 applied to do the high-resolution spectrum simulation to further reduce time-costs, which can
427 obtain high accuracy results with hundred-fold time reduction. The results of the EPIC
428 simulation measurements are consistent with theoretical analysis.

429 Based on the EPIC simulation measurements, we derived a series of coefficients from
430 various solar zenith angles for the analytic EPIC equations. Using these coefficients, we
431 performed CTP retrieval for real EPIC observation data. We have two kinds of retrieval results:
432 baseline CTP and retrieved CTP. The baseline CTP is similar to the effective CTP in Yuekui et
433 al., (2012), which does not consider cloud penetration. The retrieved CTP is derived by solving
434 the analytic equation, with consideration of the in-cloud and below-cloud interactions. Compared
435 to the effective CTP provided by NASA ASDC L2 data, the baseline CTP value at A-band is
436 slightly higher, but the baseline CTP value at B-band is substantially higher. The retrieved CTP
437 for both oxygen A- and B- bands is smaller than the related baseline CTP. At the same time,
438 compared to the oxygen A-band, both baseline CTP and retrieved CTP at oxygen B-band is
439 obviously larger.

440 **Acknowledgements**

441 This work was supported partially by NASA's Research Opportunities in Space and Earth
442 Science (ROSES) program element for DSCOVR Earth Science Algorithms managed by Dr.
443 Richard Eckman, by the National Science Foundation (NSF) under contract AGS-1608735; and
444 by the National Oceanic and Atmospheric Administration (NOAA) Educational Partnership
445 Program with Minority Serving Institutions cooperative agreement #NA11SEC4810003.

446

447 **Reference**

- 448 Chandrasekhar, S.: Radiative transfer. Dover, New York, 1960.
- 449 Chou, M.D. and Kouvaris, L.: Monochromatic calculations of atmospheric radiative transfer due
450 to molecular line absorption. *Journal of Geophysical Research: Atmospheres*, 91(D3), pp.4047-
451 4055, 1986.
- 452 Clough, S. A., Shephard, M. W., Mlawer, E. J., Delamere, J. S., Iacono, M. J., Cady-Pereira, K.,
453 Boukabara, S., and Brown, P.D.: Atmospheric radiative transfer modeling: a summary of the
454 AER codes, Short Communication, *J. Quant. Spectrosc. Ra.*, 91,233–244, 2005.
- 455 Daniel, J.S., Solomon, S., Miller, H.L., Langford, A.O., Portmann, R.W. and Eubank, C.S.:
456 Retrieving cloud information from passive measurements of solar radiation absorbed by
457 molecular oxygen and O₂-O₂. *Journal of Geophysical Research: Atmospheres*, 108(D16), 2003.



- 458 Davis, A.B., Merlin, G., Cornet, C., Labonnote, L.C., Riédi, J., Ferlay, N., Dubuisson, P., Min,
459 Q., Yang, Y. and Marshak, A.: Cloud information content in EPIC/DSCOVR's oxygen A-and B-
460 band channels: An optimal estimation approach. *Journal of Quantitative Spectroscopy and*
461 *Radiative Transfer*, 216, pp.6-16, 2018a.
- 462 Davis, A.B., Ferlay, N., Libois, Q., Marshak, A., Yang, Y. and Min, Q.: Cloud information
463 content in EPIC/DSCOVR's oxygen A-and B-band channels: A physics-based approach. *Journal*
464 *of Quantitative Spectroscopy and Radiative Transfer*, 220, pp.84-96, 2018b.
- 465 Davis, A.B. and Marshak, A.: Space–time characteristics of light transmitted through dense
466 clouds: A Green's function analysis. *Journal of the atmospheric sciences*, 59(18), pp.2713-2727,
467 2002.
- 468 Duan, M., Min, Q. and Li, J.: A fast radiative transfer model for simulating high-resolution
469 absorption bands. *Journal of Geophysical Research: Atmospheres*, 110(D15), 2005.
- 470 Ferlay, N., Thieuleux, F., Cornet, C., Davis, A.B., Dubuisson, P., Ducos, F., Parol, F., Riédi, J.
471 and Vanbauce, C.: Toward new inferences about cloud structures from multidirectional
472 measurements in the oxygen A band: middle-of-cloud pressure and cloud geometrical thickness
473 from POLDER-3/PARASOL. *Journal of Applied Meteorology and Climatology*, 49(12),
474 pp.2492-2507, 2010.
- 475 Fischer, J. and Grassl, H.: Detection of cloud-top height from backscattered radiances within the
476 oxygen A band. Part 1: Theoretical study. *Journal of Applied Meteorology*, 30(9), pp.1245-1259,
477 1991.
- 478 Gordon, I.E., Rothman, L.S., Hill, C., Kochanov, R.V., Tan, Y., Bernath, P.F., Birk, M., Boudon,
479 V., Campargue, A., Chance, K.V. and Drouin, B.J.: The HITRAN2016 molecular spectroscopic
480 database. *Journal of Quantitative Spectroscopy and Radiative Transfer*, 203, pp.3-69, 2017.
- 481 Holdaway, D. and Yang, Y.: Study of the effect of temporal sampling frequency on DSCOVR
482 observations using the GEOS-5 nature run results (Part II): Cloud Coverage. *Remote*
483 *Sensing*, 8(5), p.431, 2016.
- 484 Ishimaru, A.: Wave propagation and scattering in random media. Wiley-IEEE-Press, New York,
485 1999.
- 486 Irvine, W. M.: The formation of absorption bands and the distribution of photon optical paths in a
487 scattering atmosphere. *Bull. Astron. Inst. Neth.*, 17, 266–279, 1964.
- 488 Ivanov, V. V., and S. D. Gutshabash, 1974: Propagation of brightness wave in an optically thick
489 atmosphere. *Phys. Atmos. Okeana*, 10, 851–863.
- 490 Koelemeijer, R.B.A., Stammes, P., Hovenier, J.W. and Haan, J.D.: A fast method for retrieval of
491 cloud parameters using oxygen A band measurements from the Global Ozone Monitoring
492 Experiment. *Journal of Geophysical Research: Atmospheres*, 106(D4), pp.3475-3490, 2001.
- 493 Kokhanovsky, A. A., Rozanov, V. V., Zege, E. P., Bovesmann, H., and Burrows, J. P.: A semi
494 analytical cloud retrieval algorithm using backscattered radiation in 0.4–2.4 μm spectral region,
495 *J. Geophys. Res.*, 108, 4008, doi:10.1029/2001JD001543, 2003.



- 496 Kuze, A. and Chance, K.V.: Analysis of cloud top height and cloud coverage from satellites
497 using the O2 A and B bands. *Journal of Geophysical Research: Atmospheres*, 99(D7), pp.14481-
498 14491, 1994.
- 499 Marshak, A., and Davis, A. (Eds.): 3D radiative transfer in cloudy atmospheres. Springer
500 Science & Business Media, 2005.
- 501 Marshak, A., Herman, J., Adam, S., Carn, S., Cede, A., Geogdzhayev, I., Huang, D., Huang,
502 L.K., Knyazikhin, Y., Kowalewski, M. and Krotkov, N.: Earth observations from DSCOVER
503 EPIC instrument. *Bulletin of the American Meteorological Society*, 99(9), pp.1829-1850, 2018.
- 504 Meyer, K., Yang, Y. and Platnick, S.: Uncertainties in cloud phase and optical thickness
505 retrievals from the Earth Polychromatic Imaging Camera (EPIC). *Atmospheric measurement*
506 *techniques*, 9(4), p.1785, 2016.
- 507 Min, Q.L., Harrison, L.C., Kiedron, P., Berndt, J. and Joseph, E.: A high-resolution oxygen A-
508 band and water vapor band spectrometer. *Journal of Geophysical Research:*
509 *Atmospheres*, 109(D2), 2004.
- 510 Min, Q., Yin, B., Li, S., Berndt, J., Harrison, L., Joseph, E., Duan, M. and Kiedron, P.: A high-
511 resolution oxygen A-band spectrometer (HABS) and its radiation closure. *Atmospheric*
512 *Measurement Techniques*, 7(6), pp.1711-1722, 2014.
- 513 O'Brien, D.M. and Mitchell, R.M.: Error estimates for retrieval of cloud-top pressure using
514 absorption in the A band of oxygen. *Journal of Applied Meteorology*, 31(10), pp.1179-1192,
515 1992.
- 516 Pandey, P., Ridder, K.D., Gillotay, D. and Van Lipzig, N.P.M.: Estimating cloud optical
517 thickness and associated surface UV irradiance from SEVIRI by implementing a semi-analytical
518 cloud retrieval algorithm. *Atmospheric Chemistry and Physics*, 12(17), pp.7961-7975, 2012.
- 519 Schuessler, O., Rodriguez, D.G.L., Doicu, A. and Spurr, R.: Information Content in the Oxygen
520 A-Band for the Retrieval of Macrophysical Cloud Parameters. *IEEE Transactions on Geoscience*
521 *and Remote Sensing*, 52(6), pp.3246-3255, 2013.
- 522 Stamnes, K., Tsay, S.C., Wiscombe, W. and Jayaweera, K.: Numerically stable algorithm for
523 discrete-ordinate-method radiative transfer in multiple scattering and emitting layered
524 media. *Applied optics*, 27(12), pp.2502-2509, 1988.
- 525 Thomas, G. E., and Stamnes, K.: Radiative transfer in the atmosphere and ocean. Cambridge
526 University Press, Cambridge, 2002.
- 527 Tilstra, L.G., Wang, P. and Stammes, P.: Surface reflectivity climatologies from UV to NIR
528 determined from Earth observations by GOME-2 and SCIAMACHY. *Journal of Geophysical*
529 *Research: Atmospheres*, 122(7), pp.4084-4111, 2017.
- 530 Van de Hulst, H. C.: Multiple Light Scattering: Tables, Formulas, and Applications. Academic
531 Press, 299 pp, 1980.
- 532 Van de Hulst H.C.: Multiple light scattering: tables, formulas, and applications. Elsevier; 2012.



- 533 Yang, Y., Marshak, A., Mao, J., Lyapustin, A. and Herman, J.: A method of retrieving cloud top
534 height and cloud geometrical thickness with oxygen A and B bands for the Deep Space Climate
535 Observatory (DSCOVR) mission: Radiative transfer simulations. *Journal of Quantitative*
536 *Spectroscopy and Radiative Transfer*, 122, pp.141-149, 2013.
- 537 Yang, Y., Meyer, K., Wind, G., Zhou, Y., Marshak, A., Platnick, S., Min, Q., Davis, A.B.,
538 Joiner, J., Vasilkov, A. and Duda, D.: Cloud products from the Earth Polychromatic Imaging
539 Camera (EPIC): algorithms and initial evaluation. *Atmospheric Measurement Techniques*, 12(3),
540 2019.